New PTCR Thermistors, Switching Current, and Electromagnetic Shielding Effectiveness from Nanosized Vanadium Sesquioxides Ceramic Reinforced Epoxy Resin Nanocomposites

Farid El-Tantawy,[1] Ahmed A. Al-Ghamdi,[2] Nadia Abdel Aal[3]

[1]*Department of Physics, Faculty of Science, Suez Canal University, Ismailia, Egypt*
[2]*Department of Physics, Faculty of Science, King Abdulaziz University, Jeddah, P.O. 80203, Jeddah 21569, Kingdom of Saudi Arabia*
[3]*Chemistry Department, Faculty of Science, Suez Canal University, Ismailia, Egypt*

Received 31 January 2008; accepted 14 August 2008
DOI 10.1002/app.29083
Published online 14 September 2009 in Wiley InterScience (www.interscience.wiley.com).

ABSTRACT: A new polymer nanocomposites of an epoxy resin matrix with randomly dispersed nano-vanadium sesquioxides (V_2O_3) in various amounts were prepared. The structure of the nanocomposites were characterized by scanning and transmission electron microscopy (SEM and TEM), X-ray diffraction, hardness, packing factor, extent of filler reinforcement, glass transition temperature, and sound velocity. The percolation threshold in the conductivity of the composites is lesser than 8 wt % and the dielectric constant can reach as high as 103. The resistivity—temperature curve of the composites shows a positive temperature coefficient (PTC) effect. The thermal stability of the composites was examined in terms of thermal gravimetry and differential scanning calorimetry (TG and DTA) and isothermal resistivity–time check. Because of the interfacial interaction among filler particles and the epoxy matrix, the nanocomposites exhibit higher thermal stability. The current–voltage–temperature curves behave as switching current. The temperature increases linearly with the applied voltage which makes this PTC nanocomposites very useful for temperature probe. Finally, electromagnetic interference shielding effectiveness (SE) values have been calculated and measured for the nanocomposites in the frequency range 1–12 GHz. It is found that the SE properties of the nanocomposite improve with increase in wt % of V_2O_3. A maximum SE of 42 dB for V20 sample at 12 GHz has been achieved. These nanocomposites are potentially useful in suppression of electromagnetic interference and reduction of radar signature. © 2009 Wiley Periodicals, Inc. J Appl Polym Sci 115: 817–825, 2010

Key words: polymer nanocomposites; microstructure; electrical properties; thermal stability; electromagnetic shielding

INTRODUCTION

Nanocomposites are a new class of materials in terms of fundamental and applied sciences. The most interesting is that the physical properties of nanostructured composite are quite different from the individual components.[1–6] In these materials one of the components has nanometer dimension. The nanocomposites of inorganic solids and organic polymers are widely studied due to their improved physical properties. Vanadium sesquioxide, V_2O_3, is a member of a large vanadium oxide family where the oxidation number of vanadium ranges from + 5 in V_2O_5 to + 2 in VO. This causes a variety of interesting structural and electronic properties, making vanadium oxides interesting both for scientific research and industrial applications.[7–12] Pure and doped V_2O_3 with very good electrical and magnetic properties is a subject of intense investigations because of their potential applications in many fields such as temperature sensors, protective and time delay switching, current regulation, sensitive to applied pressure and catalysts.[8–16] A variety of crystal phases exist in the vanadium-oxygen system, a number of which display dramatic changes in electronic, magnetic, and optical properties associated with phase transitions. On the other hand, the dispersion of conductive phase within an insulating matrix, affects the overall performance of the heterogeneous system.[17] Their electrical performance is directly related to the permittivities and conductivities of their constituents, the volume fraction of filler, size and its shape of particles, aspect ratio of the filler, interface adhesion among filler and matrix processing parameters, and others.[18–22] Because of its foremost properties such as high conductivity to weight ratio, intriguing electrical properties,

Correspondence to: F. El-Tantawy (faridtantawy@yahoo.com).

flexibility and reasonably facile processibility, conducting polymer is potentially useful in thermistors, switching voltage, gas sensor, antistatic charge and electromagnetic shielding of electronic circuit and microwave absorbing screen coating.[23–27] The electromagnetic radiation is one of the unfortunate byproducts of the rapid proliferation of electronic devices, specifically due to the rapid development of 1–5 GHz electronic and telecommunication systems, such as: cellular phones, wireless internet, LAN system or "Bluetooth" devices and electronic equipment operating at 5V.[26–32] These radiations interfere with household appliances and may generate disastrous effects in large-scale computers. Therefore the importance of EMI shielding relates to the high demand of today's society on the reliability of electronics since they reduce or suppress the electromagnetic noise and the rapid growth of radio frequency radiation sources.[32] The aim of the present study is to present a new data on the influence of V_2O_3 on the network structure, electrical and electromagnetic properties of epoxy nancomposites.

PREPARATION OF V_2O_3 NANOPARTICLES

V_2O_3 nanoparticles were synthesized by heat treating sol-gel derived vanadium oxide nanopowder in reducing atmospheres. In a typical procedure, 1.0 g of V_2O_5 powder was dissolving in 30 mL of 30% H_2O_2 solution under vigorous magnetic stirring at room temperature. Red brown viscous gels are formed within 3 days by heating the solution at 65°C with controlled pH around 2.0 by adding H_2O_2.[33–40] V_2O_3 powders were formed by heating the V_2O_5 gel in a 5% hydrogen-95% argon gas mixture at 850°C for 4 h. After being dried in vacuum at 50°C for 24 h, the final black powder products were obtained. Figure 1(a) depicts the TEM micrograph of the as-prepared V_2O_3 powder. It can be seen that the sample consists of particles with average grain sizes of 23.3 ± 1.6 nm. In Figure 1, (b) is the selected area electron diffraction (SAED) pattern of V_2O_3, which is consistent with the high crystallinity of the sample.

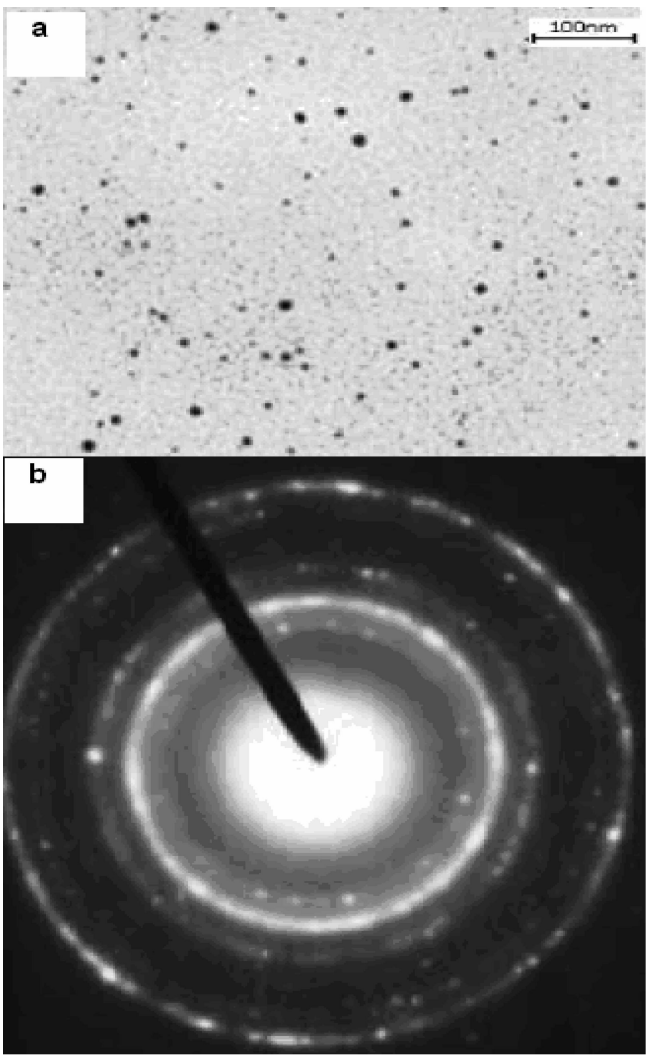

Figure 1 (a) depicts the TEM micrograph and (b) the selected area electron diffraction (SAED) pattern of the as-prepared V_2O_3 powder.

Preparation of nanocomposites

The polymer used in this investigation was a commercial epoxy resin (type 828) and hardener (type B002W) supplied by (Yuka shell epoxy chemical, Tokyo, Japan). A stoichiometric resin/hardening ratio 100 : 20 by weight was used according to the manufacturer's data sheets. V_2O_3 powder with particle size of about 23 nm is prepared as the above. Several batches of epoxy-V_2O_3 weight ratios were considered: 90 : 10, 95 : 15, and 80 : 20, respectively, and abbreviated as V10, V15, and V20, respectively. The green epoxy-hardener with different content of filler was prepared by centrifuging mixer at 4000 rpm for 2 min at room temperature. The bulk samples of composite were obtained by casting the green composites on Teflon mold and placed in an electrical oven that was preheated to 60°C for 30 min. Then, the epoxy-filler composites were cured under hot uniaxial pressure 150 KN/m^2 at 100°C for 2 h. The morphology of composites was analyzed by using a scanning electron microscopy (SEM, JSM-5310 LVB, JEOL). The specimens were coated with carbon using a vacuum evaporator (JEOL, GEE 500). The transmission electron microscopy (TEM) images and the SAED pattern were taken with a JEOL, GEE 500 transmission electron microscope. X-ray powder diffraction (XRD) patterns were recorded on a Japan Rigaku X-ray diffractometer with Cu K_∞ radiation (λ = 1.54178 Å). Thermogravimetric analysis (TGA) and differential thermal analysis was carried on a Shimadzu TGA-50H thermogravimeter analyzer and

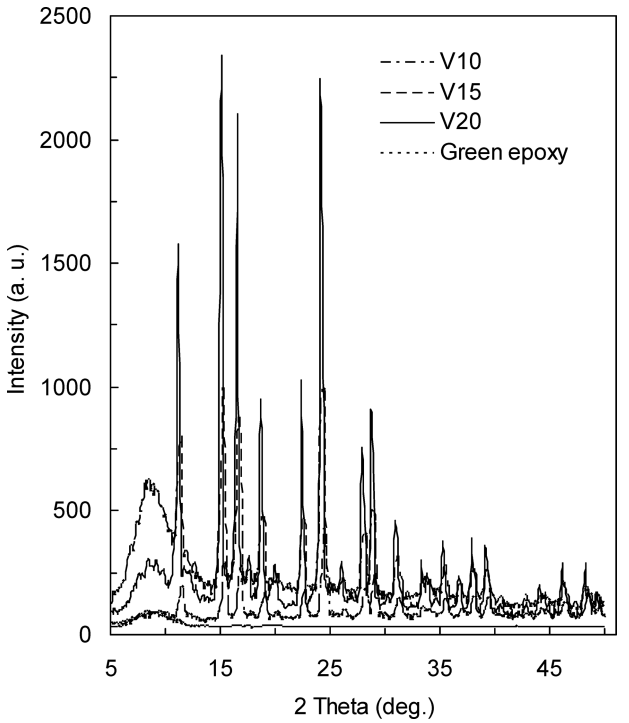

Figure 2 The room temperature XRD patterns of green epoxy and epoxy/V_2O_3 samples with different compositions.

the sample was heated from room temperature to 600°C at a rate of 10°C/min in a steady flow of nitrogen. A Shore D Hardness (H_v) was determined using a universal testing machine (ASTM D 2240 78, Osaka, Japan). The sound velocity was measured using an ultrasonic flaw detector of type Krautkramer-Branson USD-10. The Adapted technique is the pulse-echo immersion technique.[4,10] The tested sample was sandwiched between two piezoelectric ceramics operating at about 8 MHz. used a transducer. Sound velocity was determined with reference to its velocity in distilled water at 20°C (1482 m/s|). DC electrical resistivity of the composites samples was measured with increase in temperature by using a two-in-line probe technique.[3] Seebeck coefficient (S) were measured using the equation: $S = \frac{\Delta V}{\Delta T}$, where ΔV is the thermo electromotive force produced across the pellet arising from the temperature difference $\Delta T = 10°C$. The dielectric properties of the composites were measured at frequency 1 kHz by using RLC Bridge (3541 Y-Hitester, Hioki, Japan). Silver paste was used to ensure a good contact of the sample surface with copper electrodes. The current-voltage (I-V) characteristic curves were measured with a precision semiconductor parameter analyser (Keithley 442 source measure unit). The EMI properties were determined by a Hewlett-Packard (Palo Alto, CA) waveguide line containing spectroanalyzer, power meter, coefficient of reflection meter, and coefficient of attenuation meter. The measurements were carried out in the frequency range 1.0–12.0 GHz.[10]

RESULTS AND DISCUSSION

Microstructure of composites

The room temperature XRD patterns of green epoxy and epoxy/V_2O_3 samples with different compositions are shown in Figure 2. Comparing with green epoxy, as shown in Figure 2, the intensity of the V_2O_3 phase increased with V_2O_3 content increase in composites. This implied that the distribution of V_2O_3 in the sample was homogenous as confirmed by SEM images of V20 sample in Figure 3. As expected, the V_2O_3 is more dispersed, sinking into epoxy matrix and forming a more continuous phase in the composites as a result of good interfacial adhesion.[1,18] It is interesting to note that the crystallinity increases with increase in loadings level as shown in Figure 4. The increase of crystallinity with increase in V_2O_3 content, indicates that the inclusion of V_2O_3 nanoparticles improves the molecular structure of epoxy resin. The degree of crystallinity (C) was calculated using the melting peaks. The formula used for this was:[2,3]

$$C = \frac{\text{Area under melting peak}}{\Delta H_f \text{ of epoxy}} \quad (1)$$

where ΔH_f is the enthalpy of melting.

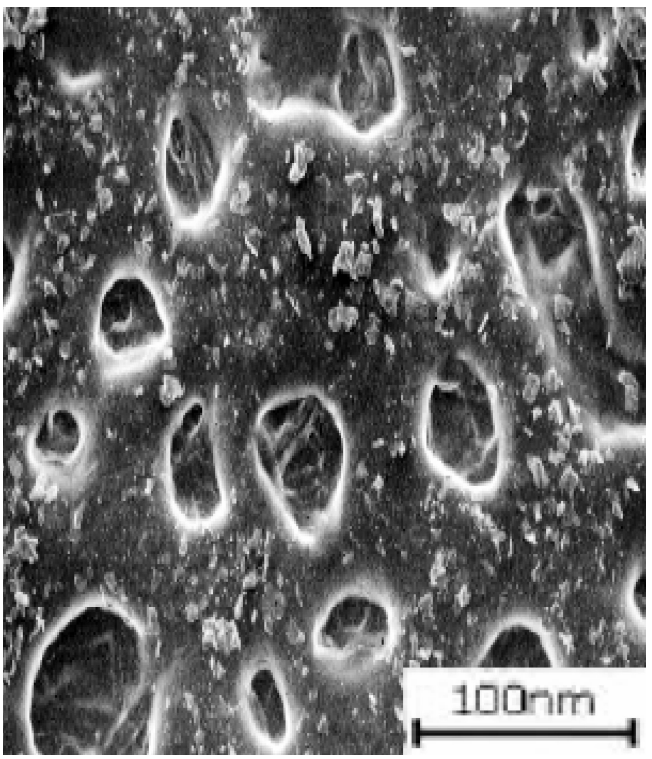

Figure 3 SEM images of V20 sample.

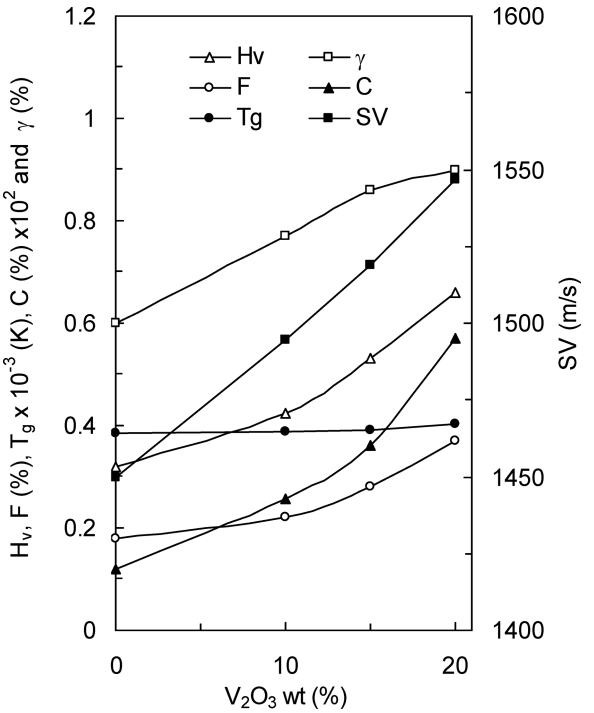

Figure 4 T_g, F, C, H_v, and SV of the epoxy/V_2O_3 nanocomposites.

In Figure 4, we observe the increase in the packing factor (F) with increase in V_2O_3 loading level which may be explained by the decrease of free volume as a function of the nanocomposite content as conformed by SEM in Figure 3. Also, the packing factor increase with increase in V_2O_3 content in the composites. This is ascribed to the strong adhesion force between neighboring chains and filler—matrix interactions into composite.[3]

The value of packing factor (F) was calculated by the equation:[20]

$$F = \frac{w_f}{V_f \rho_f} \tag{2}$$

where w_f is the weight of filler, and V_f is the volume of filler in the cylinder after vibrational compression at frequency 50 Hz and the amplitude 0.7 mm and ρ_f is the density of filler particles.[2,3]

It is realized that the extent of filler reinforcement (γ) increases with increase of V_2O_3 in epoxy matrix as shown in Figure 4. This is attributed to the integrated interfacial bonding and good wettability between filler and matrix due to the higher surface area of the V_2O_3 particles. The extent of filler reinforcement (γ) on epoxy composites can be determined as:[10]

$$\left(\frac{V_s}{V_1}\right) = 1 - \gamma\left(\frac{\phi}{1-\phi}\right) \tag{3}$$

where ϕ is the content of filler (wt %), V_1 is the volume fraction of filler and V_s is the volume fraction of epoxy in the swollen gel and is given by:[10]

$$V_s = \frac{(w_1/\rho_1)}{(w_1/\rho_1) + (w_2/\rho_2)} \tag{4}$$

where w_1 and w_2 are the weights of dry sample and solvent respectively, ρ_1 and ρ_2 are the composite and solvent densities respectively.

The glass transition temperature (T_g) as a function of V_2O_3 content is depicted in Figure 4. The T_g yields the relative stiffness, i.e., the higher T_g, the greater the polymer chain stiffness. In addition, T_g increased also is due to a decrease of thermal stress across the epoxy domains, attributed to differences in thermal expansion coefficients of composites, resulting in a positive pressure of the epoxy domains.[9–12] This is also associated with a decrease of free volume of the epoxy component and therefore with a decrease of motion ability of the epoxy molecules as confirmed by the hardness resulted in Figure 4. Hardness (H_v) increased with increase in V_2O_3 content as shown in Figure 4. This is ascribed to V_2O_3 particles reduced the creep of epoxy matrix and therein led to enhance the network structure stability within the epoxy matrix.[10] For further confirmation the above facts, the sound velocity (SV) as a function of V_2O_3 content is studied as shown in Figure 4. The sound velocity increases with increase in V_2O_3 in the composite. This is expected, as both the crosslinking density and interfacial adhesion in the samples will increase with increase in V_2O_3 content, leads to an increase of the sound velocity. On the other hand the increase of the sound velocity can be ascribed to the facile mobility carriers and the filler-polymer interaction, which induces the rigidity of the polymer chains.[2,10] This reflects the chain connectivity and interfacial adhesion increases in the composites with increase in V_2O_3 content.

Static electrical properties

The volume resistivity of the epoxy/V_2O_3 composites as a function of the weight percentage of the V_2O_3 is shown in Figure 5. An insulator—to conductor transition is observed when the V_2O_3 concentration increases. This plot shows a typical percolation phenomenon. When the amount of V_2O_3 reaches 8 wt % the resistivity of the composite is lower than that of green epoxy (conductivity of green epoxy = 10^{-13} S/m) by 16 orders of magnitude. As the amount of V_2O_3 increases, conductive networks appear in the material and the macroscopic conductivity is sharply increases.[7] Further, the reduction of resistivity with the increase of conductive filler content is attributed to the enhanced mobility of charge carriers. The increase of conductive phase content results in smaller intermolecular distance between conductive sites. This leads to the decreasing electrical resistivity of the whole composites. It is

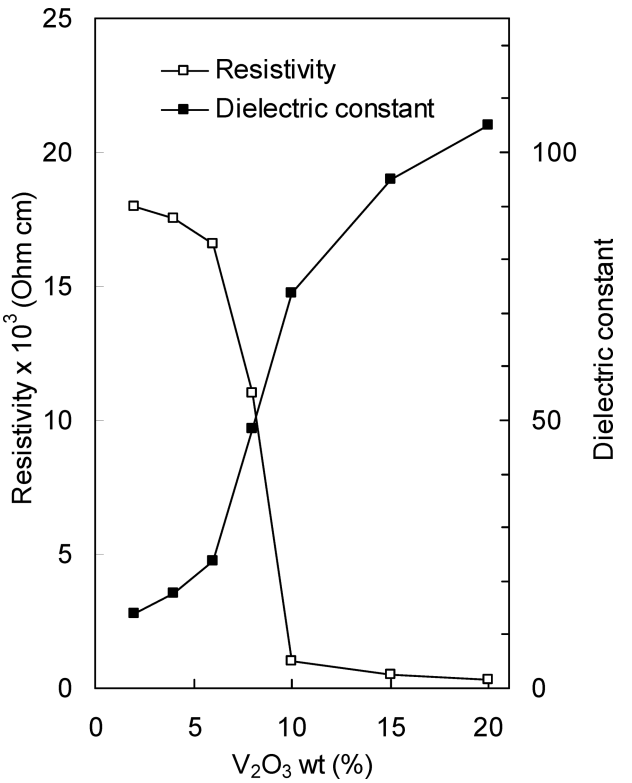

Figure 5 The volume resistivity and dielectric constants of the epoxy/V_2O_3 nanocomposites as a function of the weight percentage of the V_2O_3 at room temperature.

interesting to note that a conductivity plateau was detected in our results and was attributed to the presence of a superstructure of flocculated filler particles.[7,24] However, the phenomena demonstrates that the percolation threshold in the conductivity of the composite is lesser than 8 wt %. The percolation theory offers the following expression to describe the dependence of resistivity on filler volume content (ϕ) in the $\phi \succ \phi_c$ region:[25]

$$\rho \approx (\phi - \phi_c)^n \tag{5}$$

where n is a critical exponent and (ϕ_c) is the critical filler content.

The calculated value of n for the composites is about 1.9. The critical exponent is in good agreement with predictions from statistical percolation theory for a three-dimensional conducting network in an insulating matrix just as with other experimental results.[2,4] Dielectric constant as a function of V_2O_3 weight percentage of the composites is plotted in Figure 5. Concurrently, beyond the percolation threshold, the dielectric constants increases strongly and diverges. Qualitatively, this phenomena can be interpreted as follows.[19] Near the percolation threshold, conductive phases are separated by thin dielectric regions. The effective surface of the condensers, which are formed by neighboring conducting phases, tends to infinity when the V_2O_3 content increases. Then the effective capacity (and consequently the dielectric constants) of the sample diverges. It is worthy to mention that, the dielectric constants reaches 102 when the weight percentage of the V_2O_3 is 20 wt %, this is 37 times that of green epoxy. This is ascribed to the interfacial polarization and chain segments mobility increases with increase in V_2O_3 into composites as confirmed above.

Applicability of composites as positive temperature coefficient thermistors

The positive increase in electrical resistivity of the epoxy/V_2O_3 nanocomposites at elevated temperatures have been utilized to design "electrical self regulating heating" materials. The resistivity—temperature characteristics of the nanocomposites is presented in Figure 6. A sharp resistivity increase is generally seen at relatively high temperature and has been termed the positive temperature coefficient (PTC) effect of resistivity. The increase of resistivity with temperature is ascribed to the increase of interaggregate distance between V_2O_3 particles and thermal expansion of epoxy matrix.[4,25] The PTC effect of resistivity is attributed to a reduction in the intergranular charge carriers transport that accompanies a change in the tunneling path at high temperature.[10]

Clearly, a closer examination of the hopping and activation energies as a function of filler content is necessary to gain insight on the conduction process.

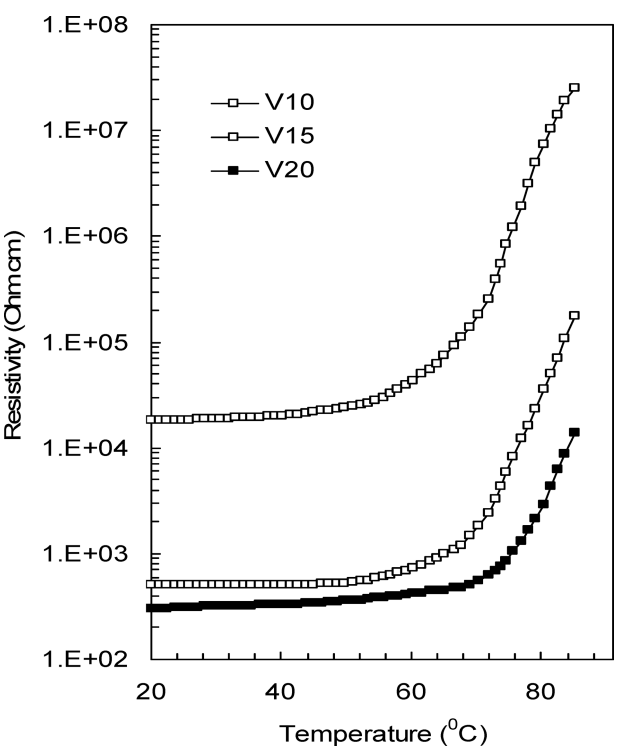

Figure 6 Resistivity-temperature plots of the nanocomposites.

The activation energy (E_a) of the conduction is given by Arrhenius relationship:[26]

$$\rho = \rho_0 e^{-\frac{E_a}{KT}} \quad (6)$$

where ρ_0 is the pre-exponential factor, K is the Boltzmann constant and T is the absolute temperature.

The values of activation energies have been calculated using least square fitting the slopes of log of resistivity versus inverse of temperature data for various concentrations in the temperature range 25–70°C and are given in Figure 7. The values of activation energies of conduction for these samples lie in the range 0.23–0.67 eV. Activation energy decreases with increase in filler content due to the increase of the charge carrier concentration and in the decrease of localized states in the band gap. As the concentration of filler increases, activation energy starts decreasing, where as resistivity decreases with filler concentration. Thus, inclusion of filler decreases the resistivity not only due to the carrier concentration but may also be due to the enhanced mobility of the charge carriers which occurs at higher loading level due to the increased interchain transport.[26] This facts is confirmed by computed the concentration of charge carriers as a function of filler content in the composites as shown in Figure 7. This is expected, as both the interchain transport and mobility carriers in the samples will increase with increase in V_2O_3 content, leads to an increase of the concentration of charge carriers. The concentration of charge carriers (N) may be evaluated on the other hand at room temperature by applying a relation containing the electrical resistivity (ρ):[3]

$$N = \frac{1}{\mu e \rho} \quad (7)$$

where e is the electron charge and μ is the drift mobility which is calculated from the Hall effect.[3]

The hopping energy (E_h) is calculated using the following relation:[27]

$$\rho T^{\frac{1}{2}} = \rho_0 e^{-\frac{E_h}{KT}} \quad (8)$$

The calculated values of the E_h as a function of V_2O_3 content is depicted in Figure 7. It is clear that the values of E_a are different from E_h in the composites. This clue support that the conduction mechanism of conductivity in the composites is controlled by tunneling mechanism.[27] To understanding the type of charge carriers in nanocomposites we measure Seebeck coefficient (S). The value of Seebeck coefficient versus filler content of nanocomposites is plotted in Figure 7. It is clear that the value of S is negative. This strong clue that the charge carriers transport in composites is controlled by electrons.

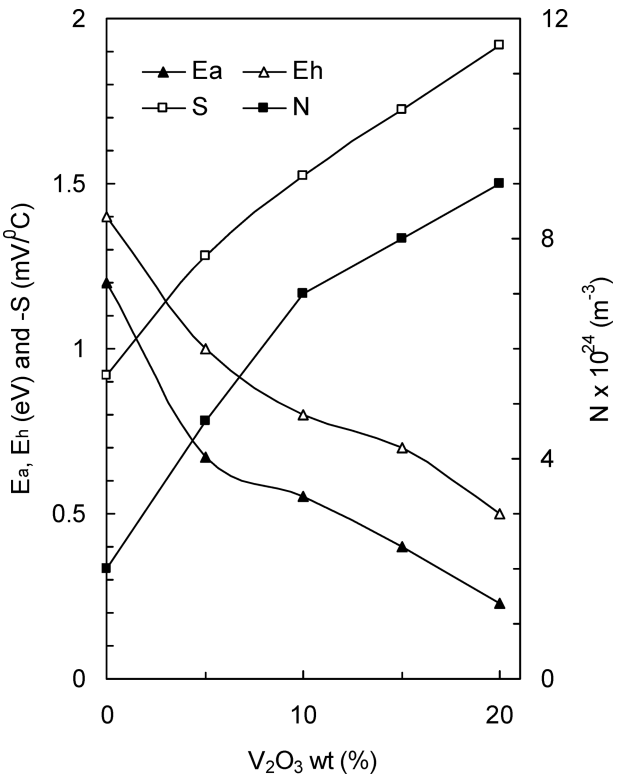

Figure 7 The values of the activation and hopping energies, Seebeck coefficient and number of charge carriers of the nanocomposites.

Thermal stability test

To explain the influence of V_2O_3 on the network structure, isothermal stability test of composites in terms of monitoring the variation of resistivity versus time at certain temperature, was conducted to obtain more information concerning interfacial bonding among filler and matrix. At first, the variation of electrical resistivity of the composites as a function of time at 50°C is monitored in Figure 8. The curve for V10 sample show two distinct steps of loss in electrical resistivity. A rapid increase in resistivity occurs up to about 10 min and thereafter a rapid decrease and then level off is observed. The initial increase of resistivity is inferred to be due to the volumetric thermal expansion of epoxy matrix.[26] For V15 and V20 samples, there is little change in resistivity at this temperature up to 20 min. Thereafter the resistivity shows a steady with time. The above results indicate that the inclusion of V_2O_3 increase the interfacial bonding among filler and matrix. Again, the epoxy charged with V_2O_3 particle has a higher thermal stability than the uncharged epoxy. This assertion is based on the analysis of the thermal gravimetry (TG) and differential scanning calorimetry (DTA) diagrams of the composites as shown in Figure 9. TG curves of green epoxy and V10 and V20 samples composites indicated that the samples

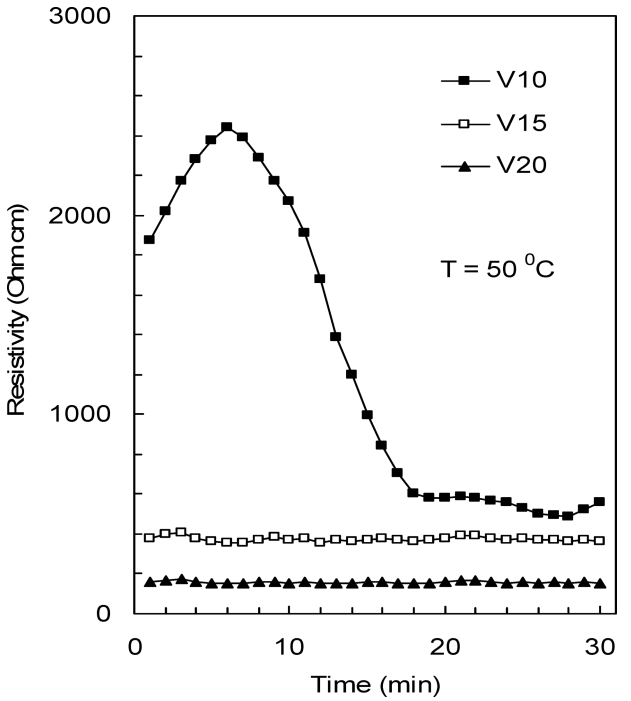

Figure 8 The variation of electrical resistivity with respect to time at 50°C.

present a higher initial degradation temperature than green epoxy. However, the onset decomposition temperatures of the composites are higher than green epoxy and are shifted towards a higher temperature range as the content of nanocomposite increase. These behaviors are assigned to the barrier effect of the filler particles and, thus, hinder the degradation process. The slight increase in the decomposition temperature with the increase of V_2O_3 content in the composite may be explained by the increase of its degree of crystallinity as supported above in Figure 4. DTA pattern show that the temperature at which thermal decomposition of the composite containing 20% V_2O_3 particle occurs is 388.90°C, compared with 315.30°C for the green epoxy. This result once again endorse the high thermal stability of nanocomposites at high V_2O_3 loading level.

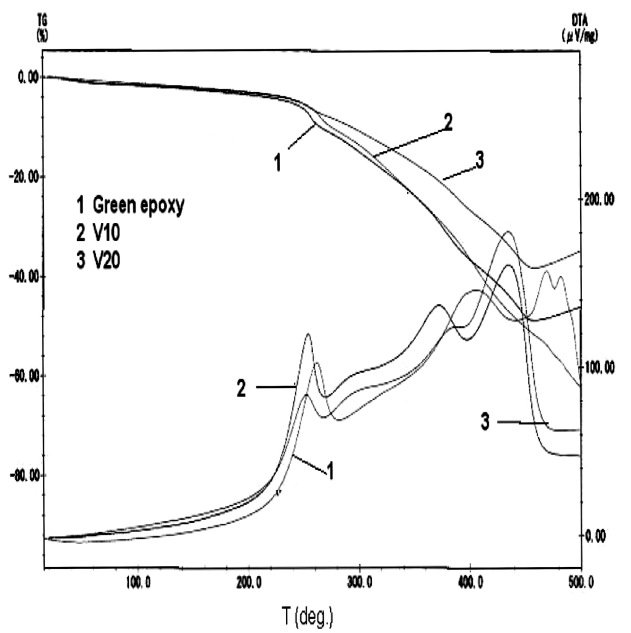

Figure 9 Thermogravimetric and differential thermal analysis of green epoxy and V_2O_3/epoxy composites in nitrogen atmosphere.

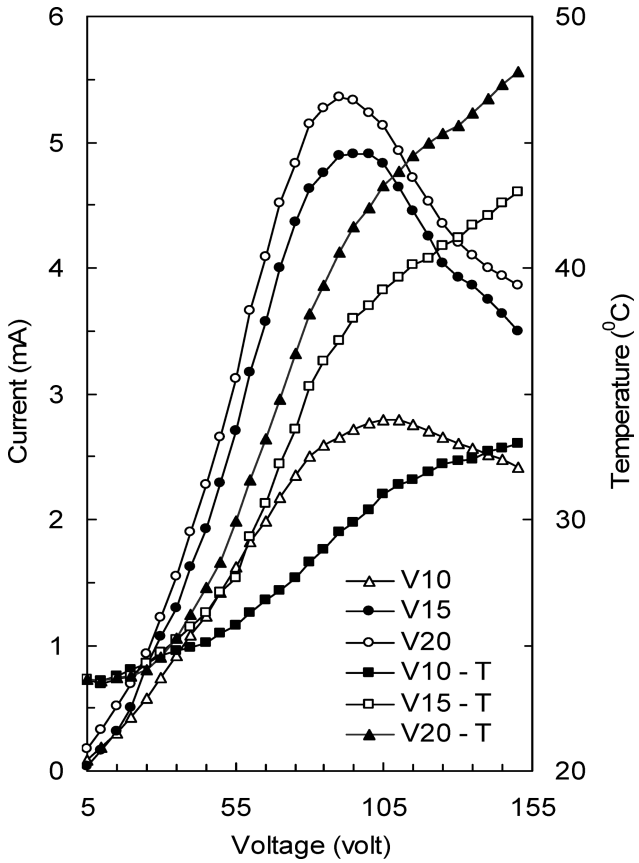

Figure 10 A typical current versus dc voltage and ultimate temperature characteristic ($I/V/T$) curve for the nanocomposites.

Applicability of composites as switching current

Figure 10 presents a typical current versus dc voltage and ultimate temperature characteristic ($I/V/$T) curve for the composites at a room temperature of 25°C. It is clear that the peak point (i.e., switching point), which is referred to as the negative resistance. In this curve, the left side of the peak point is an Ohmic region (i.e., linear region), whereas the right side is a varistor region. In the Ohmic region, a steady-state operating condition is maintained. In this condition, the composite is in thermal equilibrium and no self-heating takes place. However, in

the varistor region, the composite becomes self-heating due to the Joule heating effect. When the voltage exceeds a certain value dependence on filler concentration, the thermal equilibrium fails and the composite quickly switches to the peak state (namely switching current). With an increase of the electric field, the behavior of I-V changes from Ohmic to non-Ohmic. This is attributed to the change in the percolation conductive network across the epoxy matrix and thermal fluctuations due to significant Joule heating that took place and nonlinearity that set in. Increasing the electric field above a certain voltage, termed, depends on filler content and leads to an increase in the Joule heating effect, and consequently increases the sample temperature and decreases the current i.e., showing negative resistance.

According to the results of the V/T experiment, the maximum temperature is 50°C for V20 sample. It is interesting to note that the variation of temperature with applied potential is linear, which makes the proposed composites a very useful for temperature probe. This implies that the proposed composite is useful for low-voltage power regulation systems, such as battery- operated motors, spark quenching, and low-voltage electronic switches.

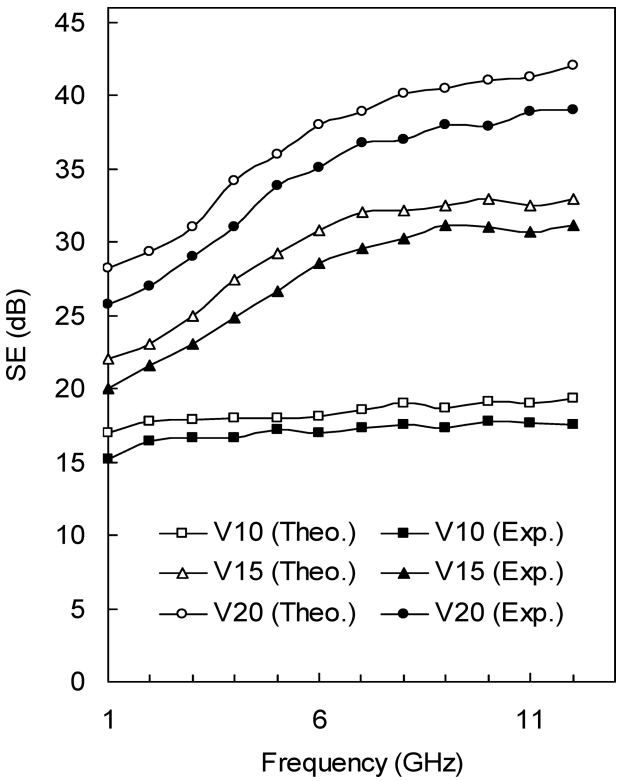

Figure 11 Comparison of theoretical and experimental data of shielding efficiency (SE) for composites as a function frequency (GHz).

Applicability of composites as electromagnetic shielding effectiveness (SE)

The shielding effectiveness is described as the attenuation of an electromagnetic signal produced by its passage through a shield and is measured as the ratio of the shield strength before and after attenuation and is determined as shielding effectiveness (SE) $\mathrm{dB} = 20\log\frac{E_t}{E_i} = 10\log\frac{P_t}{P_i}$, where E and P are the electrical field strength and power respectively. According to electromagnetic shielding effect theory,[30–32] the mechanisms of SE shielding are consists of reflection, absorption and multiple reflection. Then,

$$\mathrm{SE(dB)} = R + A + M \tag{9}$$

where R is the reflection loss at the material surface, A the absorption loss within the material and M is the internal reflection loss at internal interfaces of material itself, which can be either positive or negative and can be neglected if $A \geq 10$ dB.[32]

R is the most important part of SE and is given by:

$$R = 20\log\left(\frac{0.462}{r\sqrt{\frac{\mu_p}{f\sigma}}} + 0.316r\sqrt{\frac{f\sigma}{\mu_p}} + 0.354\right) \tag{10}$$

where r is the distance from the emission source to the shielding material, f is the incidental frequency of the electromagnetic wave, μ_p is the magnetic transmissivity, and σ is the electrical conductivity.

A is also the significant part of SE and expressed as below:

$$A = 3.34 \times 10^{-3} h\sqrt{f\mu_p\sigma} \tag{11}$$

where h is the sample thickness.

The value of the third part M is usually very small and related closely with A as:

$$M = 20\log(1 - 10^{-0.1A})\mathrm{dB} \tag{12}$$

The calculated electromagnetic shielding effectiveness (SE) (in decibels, dB) for V_2O_3/epoxy nanocomposites have been compared with measured SE as a function of frequency (GHz) in Figure 11. The shapes of both experimental and theoretically calculated SE are similar. Hence, this difference between the theoretical and measured values is expected. These differences in the measured and calculated values of SE may be further attributed to the surface irregularity of absorber sample, gap between the sample and wave-guide dimensions, air gap between sample and metal short, certain voids present in the sample as confirmed by SEM image before, etc.[18,28] High SE attenuation values ($\sim$ 42 dB), in the frequency range of 1–12 GHz, were

obtained when the composites contained 20 wt.% of the V_2O_3/epoxy nanocomposite (V20). Also the composite containing 15 wt.% of nanocomposite (V15) presents SE attenuation values between 22 and 33 dB in the frequency range of 1–12 GHz. In this case, the composite exhibits a broadband behavior, with microwave radiation absorption. Hence, the reflectivity properties of epoxy conducting composite depend on composite composition and microstructure attained after processing. In this case, the V_2O_3/epoxy nanocomposite agglomerates, between the resin phases, act on the wave-matter interaction.[17,29] This shows that these conducting V_2O_3/epoxy nanocomposite are an effective absorber in the microwave range. In addition, the V_2O_3/epoxy nanocomposite (V10) present lower microwave absorbing properties, between 1 and 12 GHz. However, the conducting nanocomposite presents a shift of the attenuation values to higher frequencies, specifically the maximum of the attenuation values occur at frequencies higher than 12 GHz.

CONCLUSIONS

The results of this research clearly show the following:

1. The network structure of the composites is strongly enhanced by the inclusion of V_2O_3 nanparticles.
2. The volume fraction dependence of electrical resistivity of the nanocomposite can be well described by the percolation theory. Moreover, the resistivity of the nanocomposites increases with increase in temperature, showing typical PTC effect.
3. The dielectric constant of nanocomposites increases slightly with increase in V_2O_3 content up to 8 wt %. Above this content, the dielectric constant increases sharply and is more than 16 orders of magnitude larger than that of green epoxy.
4. I-V-T characteristics are observed to non-Ohmic at high voltage and show certain kind of switching effect. The negative resistance after switching voltage is generated by thermal fluctuations due to significant Joule heating. Epoxy-V_2O_3 nanocomposites can be used as heating devices for consumer products and temperature probe with good thermal stability.

References

1. Mahmoud, E. W.; Hafez, M.; Abdel-Aal, N.; El-Tantawy, F. Polym Int 2008, 57, 35.
2. Todorova, Z.; Dishovsky, N.; Dimitrov, R.; El-Tantawy, F.; Abdel-Aal, N.; Al-Hajry, A.; Bououdina, M. Polym Compos 2008, 29, 109.
3. Abdel-Aal, N.; El-Tantawy, F.; Al-Hajry, A.; Bououdina, M. Polym Compos 2008, 29, 125.
4. El-Tantawy, F.; Abdel-Kader, M.; Kaneko, F.; Sung, Y. K. Eur Polym J 2004, 40, 415.
5. Glauciane, N. B.; Carlos, A.; Brunello, Carlos, F. O. G.; Herenilton, P. O. J Solid State Chem 2004, 177, 960.
6. Kolczewski, C.; Hermann, K.; Guimond, S.; Kuhlenbeck, H.; Freund, H. J. Surf Sci 2007, doi:10.1016/j.susc. 09.033.
7. Patricia, A. M.; Shekhar, G.; Leonel, P. G.; Jacob, O. B.; Elliott, B. S.; Jurgen, M. H. Thin Solid Films 2007, 515, 3421.
8. Zeheng, Y.; Peijun, C.; Luyang, C.; Yunle, G.; Liang, S.; Aiwu, Z.; Yitai, Q. J Alloys Compd 2006, 420, 229.
9. Liuya, W.; Xiangfeng, C.; Deming, L.; Chenmou, Z.; Xiao-Ming, C. J. Mater Sci Eng B 2006, 131, 116.
10. El-Tantawy, F.; Kamada, K.; Ohnabe, H. Mater Lett 2002, 57, 242.
11. Wang, H.; Zhang, H.; Chen, G. Compos A 2007, 38, 2116.
12. Abthagir, P. S.; Saraswathi, R. Thermochim Acta 2004, 424, 25.
13. Sadia, A.; Vazid, A.; Zulfequar, M.; Haq, M. M.; Husain, M. Curr Appl Phys 2007, 7, 215.
14. Stephen, H. F. J Appl Polym Sci 199, 37, 1899.
15. Lorraine F. F.; Jaime, C.; Grunlan, J. S.; Gerberich, W. W. Colloids Surf A 2007, 311, 48.
16. Josef, Z. K.; Bala, S. V.; Karl, S.; Wolfgang, B. Compos Sci Technol 2007, 67, 922.
17. Chiung-Chih, L.; Woei-Shyong, L.; Chang-Chun, S.; Wen-Hwa, W. Ceram Int 2008, 34, 131.
18. Lafosse, X. Synth Met 1995, 68, 227.
19. Chung, D. D. L. Carbon 2001, 39, 279.
20. Mauro, A. S. O.; Olacir, A. A.; Roselena, F.; Mirabel, C. R.; Marco-A, D. P. Synth Met 2006, 156, 1249.
21. Abbas, S. M.; Dixit, A. K.; Chatterjee, R.; Goel, T. C. J. Mater Sci Eng B 2005, 123, 167.
22. Dhawan, S. K.; Singh, N.; Venkatachalam, S. Synth Met 2002, 129, 261.
23. Lai, Z. Elementary Theory of Electromagnetic Shielding; Atomic Energy Publishing Company: Beijing, 1993.
24. Sukanta, D.; Ashis, D.; De, S. K. Solid State Commun 2006, 137, 662.
25. Chih-Kuo, L.; Chen-Che, T. Sens Actuators A 2005, 121, 443.
26. Phang, S. W.; Rusli, D.; Abdullah, M. H. Thin Solid Films 2005, 477, 125.
27. Bliznyuk, V. N.; Baig, A.; Singamaneni, S.; Pud, A. K.; Fatyeyeva, Y.; Shapoval, G. S. Polymer 2005, 46, 11728.
28. El-Tantawy, F. J Appl Polym Sci 2005, 97, 1125.
29. Wang, T.; Chen, G.; Wu, C.; Wu, D. Prog Org Coat 2007, 59, 101.
30. Chen, G.; Wu, C.; Weng, W.; Wu, D.; Yan, W. Polymer 2003, 44, 1781.
31. Chen, G.; Weng, W.; Wu, D.; Wu, C.; Lu, J.; Wang, P; Chen, X. Carbon 2004, 42, 753.
32. Das, N. C.; Khastgir, D.; Chaki, T. K.; Chakraborty, A. Compos A 2000, 31, 1069.
33. Bahgat, A. A.; Ibrahim, F. A.; El-Desoky, M. M. Thin Solid Films 2005, 489, 68.
34. Stupp, S. I.; Lebonheur, V.; Walker, K.; Li, L. S.; Huggins, K. E.; Keser, M. A. Science 1997, 276, 384.
35. Adler, D. Rev Mod Phys 1998, 40, 714.
36. Begishev, A. R.; Legnat'ev, A. S.; Kapaev, V. V.; Mokerov, V. G. Sov Phys Tech Phys 1979, 24, 1263.
37. El-Tantawy, F. J Appl Polym Sci 2005, 98, 2226.
38. Rozgonyi, G. A.; Hensler, D. H. J Vac Sci Technol A 1968, 5, 194.
39. Balberg, I.; Torkman, S. J Appl Phys 1975, 46, 2111.
40. Gossard, A. C.; Menth, A.; Warren, W. W.; Remeika, J. P. Phys Rev B 1971, 3, 3993.